NeuroImage 117 (2015) 103–113

Contents lists available at ScienceDirect

NeuroImage

journal homepage: www.elsevier.com/locate/ynimg

Global features of functional brain networks change with contextual disorder

Michael Andric [a,*], Uri Hasson [a,b]

[a] Center for Mind/Brain Sciences (CIMeC), The University of Trento, Rovereto, TN, Italy
[b] Department of Psychology and Cognitive Sciences, The University of Trento, Rovereto, TN, Italy

ARTICLE INFO

Article history:
Received 7 January 2015
Accepted 9 May 2015
Available online 16 May 2015

ABSTRACT

It is known that features of stimuli in the environment affect the strength of functional connectivity in the human brain. However, investigations to date have not converged in determining whether these also impact functional networks' global features, such as modularity strength, number of modules, partition structure, or degree distributions. We hypothesized that one environmental attribute that may strongly impact global features is the temporal regularity of the environment, as prior work indicates that differences in regularity impact regions involved in sensory, attentional and memory processes. We examined this with an fMRI study, in which participants passively listened to tonal series that had identical physical features and differed only in their regularity, as defined by the strength of transition structure between tones. We found that series-regularity induced systematic changes to global features of functional networks, including modularity strength, number of modules, partition structure, and degree distributions. In tandem, we used a novel node-level analysis to determine the extent to which brain regions maintained their within-module connectivity across experimental conditions. This analysis showed that primary sensory regions and those associated with default-mode processes are most likely to maintain their within-module connectivity across conditions, whereas prefrontal regions are least likely to do so. Our work documents a significant capacity for global-level brain network reorganization as a function of context. These findings suggest that modularity and other core, global features, while likely constrained by white-matter structural brain connections, are not completely determined by them.

Introduction

The extent to which functional brain connectivity reorganizes with context, and whether any such reorganization is systematic or random is a topic of much recent debate. There is ample work documenting effects of the external environment on connectivity-strength between regions. For example, connectivity has been shown to vary depending on the task performed (e.g., Mennes et al., 2013) and to adjust before task execution to match task features (Ekman et al., 2012). Connectivity is affected also by subtle manipulations, such as changes to linguistic features during listening (e.g., Hasson et al., 2009; Chow et al., 2014). The content of internally generated ("endogenous") thoughts, absent exogenous stimuli, also modifies functional connectivity (e.g., Preminger et al., 2011; Doucet et al., 2012). Thus, both exogenous tasks and endogenous states can produce robust and systematic connectivity changes among brain systems.

What is less clear is whether functional connectivity networks maintain global features across different environments, or conditions. As we review below, the literature addressing this question is relatively small, typically involves extreme contrasts (e.g., task vs. rest or sleep states), and offers divergent results. In an early MEG investigation of this issue, Bassett et al. (2006) found that task performance did not significantly impact networks' global topological parameters, such as path length, clustering coefficient, and degree distributions, but instead affected inter-regional connection strength. In another MEG study, Nicol et al. (2012) also documented changes to local — but not global — connectivity parameters, in this case during responses to regular and deviant auditory tones. These studies suggested that connectivity networks could remain task invariant. However, Kitzbichler et al. (2011) found that some global network connectivity parameters within particular frequency bands changed as a function of people's task-related cognitive effort. We note that these three studies derived networks from MEG sensor time series (rather than source space); beyond offering limited information about the brain anatomy underlying these networks, constructing connectivity networks from MEG sensor space is susceptible to measuring the same brain sources across different sensors. (Also, if a single source is measured at 2 remote sensors in one condition but not the other, this may be interpreted as a change in network structure.)

fMRI studies have also revealed mixed findings. A recent study (Betti et al., 2013) that combined MEG and fMRI to quantify connectivity changes during rest vs. movie viewing did not find task-related effects

* Corresponding author at: Via Delle Regole, 101, Mattarello, TN, Italy.
E-mail address: andric.michael@gmail.com (M. Andric).

http://dx.doi.org/10.1016/j.neuroimage.2015.05.025

on network topography, but did document changes to MEG frequency power distribution. Uehara et al. (2014) examined functional network organization during sleep and wakefulness and found no differences in network modularity or number of modules. Stanley et al. (2014) found no impact of working memory load on global features related to modular organization. Moussa et al. (2011) quantified connectivity during rest, visual, and multisensory stimulation and documented no task effect on 6 different global features, including modularity and mean degrees. This study, however, did identify more local effects, evident by spatial changes in the extent of functional modules' overlap with auditory and sensory cortices. Similarly, Bray et al. (2014) also found that large-scale network organization maintained across conditions (rest and task states), though certain regions on the spatial periphery of these large-scale networks switched network arrangement with task. Finally, two other fMRI studies that did not study whole-brain (large-scale) connectivity documented condition-related changes in sub-networks of larger scale ones (e.g., Fornito et al., 2012; Cole et al., 2013).

Given these mixed prior findings on the context-dependence of functional connectivity's global features, our over-arching goal in the current work was to address whether, and under what conditions, changes in connectivity mark essential changes in the brain's network topology. First, we aimed to determine if variations in naturalistic contexts, absent of executive task demands, are associated with systematic changes to core global topological features, such as modularity strength, number of modules, partition structure, and node degree distributions. As reviewed above, in prior studies these features were studied by comparisons among different tasks or comparisons of task to rest. These manipulations direct participants' efforts and attention to specific stimulus features, and 'context' is operationally defined as a stimulus–response mapping during a block of trials.

Departing from these models, we used a passive listening paradigm. Our experimental conditions were identical in sensory/physical features and (lack of) task demands, differing only in long-term statistical relations (mean regularity; i.e. entropy) of the input conditions. Such input regularity manipulations have long been known to impact the tendency to mind-wander during listening (Antrobus, 1968) and to affect the aesthetic appraisal of the input (Vitz, 1966). Thus, manipulating steady-state regularity is a subtle but potentially powerful implicit manipulation for inducing large-scale connectivity changes. In fact, connectivity changes in striate and visual cortex have been linked to associative learning of cue-target predictability (den Ouden et al., 2009, 2010). Thus, we aimed to understand whether manipulations of input regularity could result in re-configuration of whole-brain networks in a way that affects global network features — even when individuals were not tasked with monitoring the stimuli at all.

Our second goal was to identify particular brain areas whose connectivity remained relatively affected or unaffected, even given changes to global connectivity. We treated each brain voxel as a node and quantified the extent to which it maintained its within-module connectivity between conditions. This allowed us to document specific brain areas for which the external environment either strongly or weakly impacted their within-module connectivity cohort.

Prefacing our results, we found that our experimental manipulation had a systematic effect on modularity strength, partition similarity, and networks' degree distributions — all considered global network features. Further, our node-level analysis showed that the experimental manipulation particularly affected prefrontal regions, which maintained only ~20% of their within-module connections between conditions, whereas regions implicated in sensory and default processes maintained a much higher proportion, suggesting greater resilience to environmental changes. Prefrontal regions also showed a significant change in overall connectivity strength as function of condition. Our findings indicate that implicit, endogenous processing is extremely potent, effecting changes to global topographic features. Importantly, however, these changes obscure a heterogeneous, non-uniform pattern of organizational changes to network module membership across the brain.

Materials and methods

Participants

Twenty-one right-handed participants (12 men, mean age = 29.9 years, SD = 9.6) from the University of Trento community took part in the study. None reported any history of neurological or psychiatric disturbance, hearing impairments, or substance abuse. One participant's data was excluded from the study because of excessive movement during the scan. Another participant's data was excluded due to low structural image quality that prevented gray-matter segmentation in the preprocessing phase of the analyses. The Ethical Review Board of the University of Trento approved the study.

Stimuli

The materials used were auditory tone sequences. Each tone in a sequence was presented for 250 ms followed by a 50 ms break. We used pure tones at 262, 294, 330, or 349 Hz, corresponding to middle "C", "D", "E", and "F" notes on the Western major scale. The tones' sequence order was determined using a first-order Markov process applied to four transition matrices with different levels of Markov entropy (Markov entropy = 0.81, 1.35, 1.56, 2.0; Fig. 1).

These four entropy levels thus marked the four experimental conditions in this study: *Highly ordered*, *Some order*, *Almost random*, and *Random*. In the *Random* condition, each tone was equally likely to appear at any point, independently of the previous sequence, i.e., there were no transition constraints. By contrast, in the other three conditions, there were increasing constraints. Note that in all conditions all tones occurred equally often over the entire series, i.e., marginal

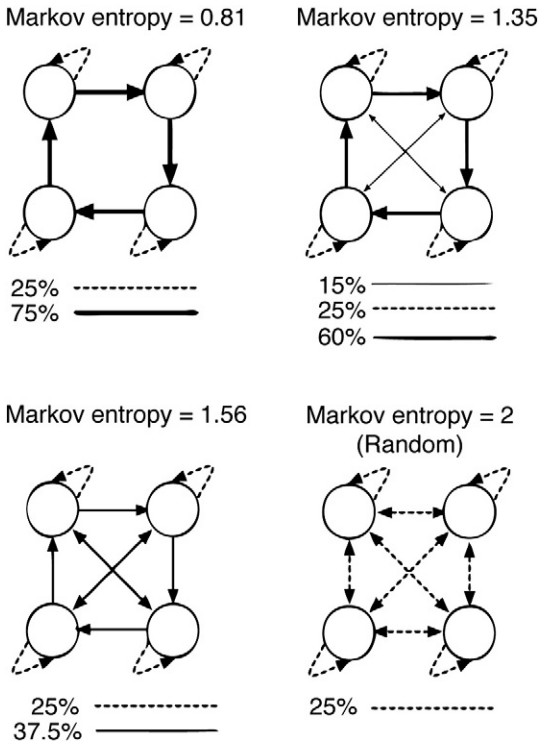

Fig. 1. Markov processes used to generate the four auditory series. Each node in the transition matrix corresponded to a pure tone. Line weights represent transition probability. The entropy of the Markov processes ranged from random (Markov entropy = 2.0) to highly ordered (Markov entropy = 0.81).

frequencies were identical and did not differentiate the series. In addition, the proportion of self-repetitions was equivalent across conditions and set at 25%. Conditions were presented in 150 s epochs, each followed by 21 s of silence. The functional run began with 22.5 s of silence. The order of conditions presented in the run was counterbalanced across participants.

Procedure

Since instructions to explicitly monitor statistical relations can interfere with implicit learning (e.g., Fletcher et al., 2005) we used a passive listening procedure without mentioning any aspect related to the structure of the series. In the MRI scanner, participants were instructed to attend to auditory stimuli presented over the headphones, while observing a fixation cross. To later mitigate the impact of physiological noise sources in the functional data we used a photoplethysmograph to collect cardiac data and a respiration belt to collect respiration data. Prior to the main experiment, a volume calibration procedure was conducted for each participant to set a volume level at which they could comfortably hear the series over the scanner noise.

Image acquisition

Images were acquired using a 4 T Bruker/Siemens system. Functional images were acquired with a single shot echo planar imaging blood oxygen level dependent (BOLD) sequence: 25 interleaved slices parallel to the AC/PC, TR = 1500 ms, TE = 33 ms, flip angle = 75°, voxel size = 4 × 4 × 4 mm, matrix = 64 × 64 mm, and slice skip factor = 0.2. We collected 471 EPI scans over a single 706.5 s run. For structural images, we used a 3D T1-weighted MPRAGE sequence to collect 176 sagittal slices, with TR = 2700 ms, TE = 4 ms, flip angle = 7°, matrix = 256 × 224, and isotropic voxel size of 1 mm. To increase the signal-to-noise ratio, for each participant, we collected two structural scans that were aligned and averaged.

Data analyses: preprocessing and construction of connectivity matrices

Single-participant preprocessing

To mitigate the impact of nuisance components on the functional data, we applied the following series of procedures. First, we spliced functional images from the individual runs to keep only those four epochs that corresponded to temporal intervals where auditory stimuli were presented. We then removed the first 10 images (15 s) of each tone-series presentation. This was done to allow for a stabilization of the BOLD response when switching from silence to auditory presentation and because any effects of regularity cannot appear until a certain number of stimuli have been presented (i.e., in the early stages, the conditions are less differentiated). This resulted in 4 time series per participant.

We applied physiological noise correction to the data following the procedure of Birn et al. (2006). To match the timing of each EPI slice acquisition, we down-sampled and phase shifted the recorded cardiac and respiratory signals to the slice-acquisition timing resolution (i.e., 16 Hz; ~3 times the physiological sampling rate). From these signals, we created 13 slice-based regressors: 4 for the cardiac series and its harmonics, 4 for the respiratory series and its harmonics, and 5 for respiration variation of time and its harmonics, using AFNI's (Cox, 1996) *retrots.m* pipeline. The variance explained by these regressors was removed with the RETROICOR procedure (Glover et al., 2000) in AFNI. To attenuate the effect of spurious signal spikes, we also despiked the time series using AFNI's *3dDespike* utility. We then spatially registered each of the 4 time series to a single reference location in the first run. To increase the temporal signal-to-noise ratio of each voxel's time series we applied a moderate 6 mm spatial smoothing given our effective voxel size (4 × 4 × 4.8 mm). Finally, we removed motion-related signal fluctuations and linear, quadratic and cubic trends via a regression model. We inspected the estimated head motion parameters for each participant and condition. Functional volumes with sudden motion in excess of 1 mm were censored in the subsequent regression — this accounted for approximately 1.5% of the data.

For each participant, we aligned the structural scan to the reference functional scan using AFNI's *3dAllineate* procedure. Gray matter masks for each participant were then created using FSL's *bet* (Smith, 2002) and *first* (Patenaude et al., 2011) tools for brain extraction and segmentation. These masks were used to extract functional data from gray matter voxels.

Construction of connectivity matrices

For each participant, we created a complete cross-correlation matrix from the time series of all voxels within a participant's gray matter mask. Across participants, the number of voxels in the mask ranged from 9044 to 12,940 (M = 10,900, SD = 886 voxels). To maintain the same number of edges (links) across experimental conditions and maintain the same proportion of connections across participants, we binarized connectivity matrices using edge density criteria. The edge density values were 5%, 12%, 15%, and 8.72%, the latter being the median edge density corresponding to what would be found if each person's connectivity matrix were binarized at a Pearson's *R* threshold of 0.5. Edge densities below 15% were not used, as those would include links where covariance was relatively weak. The resulting binary matrix, per person, formed the basis for all subsequent analyses. We created these connectivity maps and performed subsequent network analyses using R code (https://sourceforge.net/p/cnari/code/HEAD/tree/trunk/projects/bct/) based on the functions in the brain connectivity toolbox (Rubinov and Sporns, 2010). The Matlab version of the toolbox was used for creating matched random networks.

Data analyses: modularity

Network modularity and number of modules across conditions

Modularity is a graph-theoretic measure for quantifying the quality of a partition. Modularity is higher the more partitioned a network is into modules that are densely connected within rather than between themselves. In the current study, we applied this measure to single-participant networks (binarized cross-correlation matrices). We used a fast-unfolding community detection method (Blondel et al., 2008) based on modularity optimization to partition individual participants' connectivity structures. While several prior fMRI studies of modularity (e.g., Chen et al., 2008; Bassett et al., 2011; Uehara et al., 2014) operated on a region-of-interest level of granularity, treating regions as nodes, voxel-level analyses are arguably more accurate (e.g., Hayasaka and Laurienti, 2010). For this reason, and because we wanted to draw conclusions with good anatomical precision, we considered individual voxels as nodes and their connections as edges.

The modularity measure (Q) we used is given in Eq. (1).

$$Q = \frac{1}{2m}\sum_{C\in Pi,}\sum_{j\in C}\left[Aij - \frac{k_i k_j}{2m}\right] \quad (1)$$

The indices i and j run over N nodes in the graph; A is the network's adjacency matrix; m is the sum total number of edges; the degree of node i is $k = \sum_j A_{ij}$; and, the index C iterates over the modules of partition P. The community detection algorithm aims to maximize Q for a given network, with the quality of the optimized partition captured by the value of Q. We applied the algorithm to the binarized connectivity matrices of the 4 conditions per participant to obtain a representative Q value per condition. Note that given the non-deterministic nature of Blondel et al.'s partition-finding algorithm, it is possible to obtain different Q values from the exact same binarized connectivity matrix. For this reason we applied the partitioning algorithm 100 times per condition per participant and, from the resulting distribution, we chose the

maximum Q value as representative of that condition per participant (following, e.g., Stanley et al., 2014). We note that across participants and conditions these sets of 100 unique solutions returned highly similar Q values (SD of solutions = .002, which is 2 orders of magnitude smaller than the maximum Q value). To examine differences between conditions we then evaluated the maximum Q values for the 4 conditions at a group-level, using a non-parametric statistical test (Friedman's test for repeated measures). Similarly, to quantify the number of modules in each condition, on the basis of the aforementioned 100 iterations per condition we determined the *number* of modules per condition, in the previously identified max-Q partition (again, defined per participant per condition).

Validation of modularity measures against random networks

Brain networks partition more strongly than random ones (Meunier et al., 2009; Bassett et al., 2011). Therefore, as a validity check (following Meunier et al., 2009; Bassett et al., 2011; Bullmore and Bassett, 2011), we examined whether Q values for the experimental data differed from those that would be found for yoked, random networks that had the same number of nodes and equivalent degree distributions but with connections randomly assigned. For each participant in each condition, we generated 100 randomized networks, set the edge density value to 5%, and applied the modularity analysis to the resulting binarized matrices. From the resulting 100 Q values the median represented the *random* Q value for a given participant/condition. Across participants, this set of Q values was compared against the Q values selected from the actual data when thresholded at 5% edge density, as defined above.

Data analyses: additional global and local metrics for between-condition differences

Partition similarity

Prefacing the findings, we found that modularity (Q) was stronger in the most random condition than in the highly ordered one. To determine whether these changes in modularity were accompanied by a structural change to network partitions we evaluated the similarity of partitions in these two conditions, using two well-established measures: the *Adjusted Rand Index* (Rand, 1971; Hubert and Arabie, 1985) and *Normalized Mutual Information* (Kuncheva and Hadjitodorov, 2004; Danon et al., 2005).

Given prior work showing that modularity maximization algorithms can converge on markedly different partitions for the same network (Good et al., 2010), we again adjusted for the stochasticity of the algorithm by examining differences between distributions. Using the 100 partitioning solutions obtained per condition, we paired 100 unique partitioning solutions in the Random and Highly ordered conditions, obtaining a partition-similarity metric for each pairing. It is this distribution (rather than a single value) that reflected the similarity of partitions in these two conditions. In addition, to define an upper bound for partition similarity across conditions we established a sampling distribution by determining partition similarity *within* a single condition. To this end, from the 100 partitions derived for the Highly ordered condition, we quantified similarity for every unique combination (n = 4950). This latter data constituted a reference distribution against which we compared the cross-condition similarity results.

Single node set consistency (SNSC)

In addition to assessing overall partition similarity, we also quantified changes in partitioning at a finer scale: the single node level. Here we focused on the extent to which different brain regions showed changes to their within-module connectivity cohort: context effects may be accompanied by either a strong or weak re-arrangement of within-module connectivity at the single node level, and it is this relative extent of change that we targeted here.

We focused on the connectivity network obtained at 5% edge density. For every node ("voxel", used interchangeably henceforth) in a module in the Random condition, we evaluated two sets of connections: Specifically, we identified all its within-module connections in the Random condition (*Random_set*) and all its within-module connections in the Highly ordered condition (*HighlyOrdered_set*). To define a measure of a voxel's within-module overlap between the two conditions (i.e., its "set consistency") we quantified the proportion of overlap between the *Random_set* and *HighlyOrdered_set* (see Eq. (2)). This captures the proportion of within-module connections in the Random condition that were also within-module connections in the Highly ordered condition. To illustrate, if node *i* was connected to 100 nodes in its module in the Random condition and of those 100 nodes, only 20 were within node *i*'s module in the Highly ordered condition, the extent of overlap would be 20%. In contrast, if node *i* maintained all its connections in the Highly ordered condition, the extent of overlap would be 100%. In each of these two conditions, we included modules that comprised at least 20 voxels.

We refer to the single-node extent of overlap as single-node set consistency: *SNSC*, as given in Eq. (2).

$$SNSC = \frac{Random\_set \cap HighlyOrdered\_set}{Random\_set} \tag{2}$$

We derived an SNSC map for each participant and combined these into a 'group-level' representation in the following way: We used the partitions with the maximal Q value, as identified for the Highly ordered and Random condition (see above). We derived SNSC maps from these partitions on a single participant level. We collapsed these individual-level SNSC maps into a single group-level map by using each voxel's median value across participants (Fig. 2).

As in prior analyses, we also derived a null distribution for the SNSC measure to determine whether the distribution of SNSC values between the Random and Highly ordered conditions would be lower than expected by chance. Since SNSC measures individual voxels' module memberships between conditions, we generated the null distribution from a single condition. Specifically, we (1) used the 100 partitioning solutions (described in section *Network modularity and number of modules across conditions*); (2) of those, we selected 50 (we were limited to 50 instead of the full set of 100 by computation time) and combinatorially crossed those to obtain 2450 'null' SNSC solutions per participant; (3) from this set of 2450 permutations we derived a representative SNSC map per participant by assigning, for each voxel, the median value of all 2450 solutions for that voxel ('participant-median map'); (4) finally, as we did for the real SNSC maps described above, we combined the individual participant-null maps into a group level representation by taking the median of each voxel across participants. This constituted a group-median null distribution of SNSC values against which we contrasted SNSC values for the Random vs. Highly ordered conditions.

Node degree distributions

The number of edges (connections) between a node and other nodes in the graph (or network) defines the node's *degree*. We examined whether the distribution of node degree values differed across conditions (again using the 5% edge density networks). Following previous studies (Achard et al., 2006; Bassett et al., 2006; Fornito et al., 2010; Hayasaka and Laurienti, 2010), for each participant in each condition we fit the degree distribution using an exponentially truncated power law function, $P(k) \sim Ak^{\alpha-1}e^{k/k_c}$. From these fits, we extracted values for the power law exponent (α), exponential cutoff point (k_c), and coefficient (A), and evaluated those parameters at the group level using a non-parametric Friedman test for repeated measures.

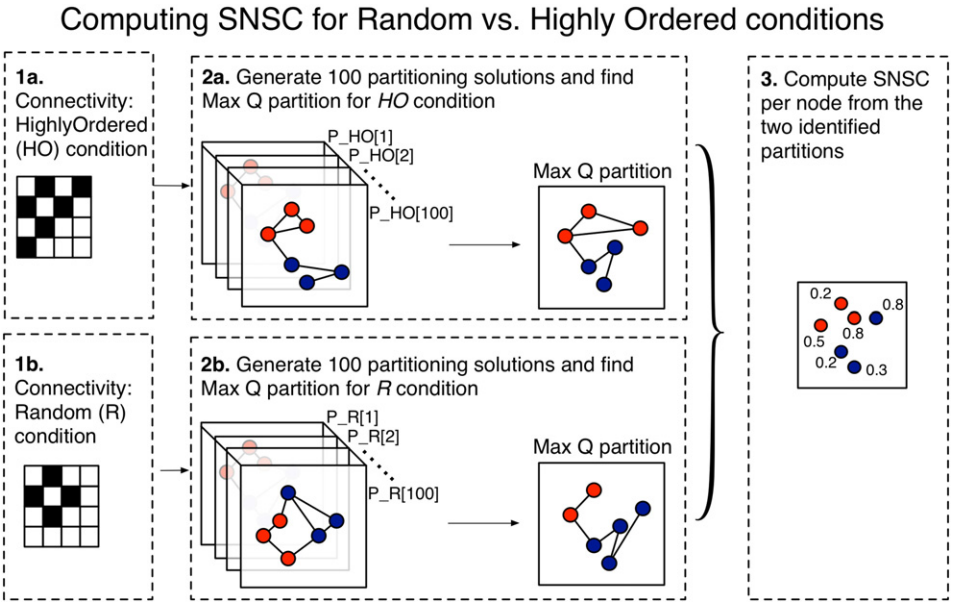

Fig. 2. Computing single node set consistency (SNSC) between the Highly ordered and Random conditions. Per participant in each of these two conditions (1a and 1b), we generated 100 modularity partition solutions (2a and 2b), in which every voxel was in a module. For each condition, the partition with the maximal *Q* was identified. For these two partitions, we calculated the proportion of within-module voxels that maintained both in Random and Highly ordered, as specified in Eq. (2) (see text) (3). This proportion defined the voxel's SNSC value. The group-level data were the median value for each voxel, across participants.

Average global (whole-brain) connectivity

In addition to the above-described measures, which focus on changes in network organization, we also examined voxel-level changes in connectivity strength. We used a voxel-wise connectivity measure (whole-brain un-weighted global connectivity; Cole et al., 2010), which was operationalized as the mean functional connectivity (Pearson's R) between a voxel and all other gray-matter voxels. For each participant, this measure returned one value per voxel per condition. These values were Fisher-Z transformed and analyzed at a group level using two orthogonal contrasts: one testing for a linear trend (.75, .059, −.179, −.63) and another testing for a U-shaped trend (.42, −.57, −.41, .56). We used cluster-based control for family-wise error rate (FWE) to identify significant clusters. We set the single voxel threshold at $p < .01$, with a volume of at least 1136 mm^3 to control for FWE of $p < .05$. We determined this via AFNI's 3dClustSim, following the algorithm of Forman et al. (1995).

Results

We first present findings showing the impact of the experimental conditions on global network features, such as modularity, partition similarity, and node degree distributions. We then report results characterizing single-node-level (voxel-level) connectivity changes, in terms of both within-modular consistency and degrees.

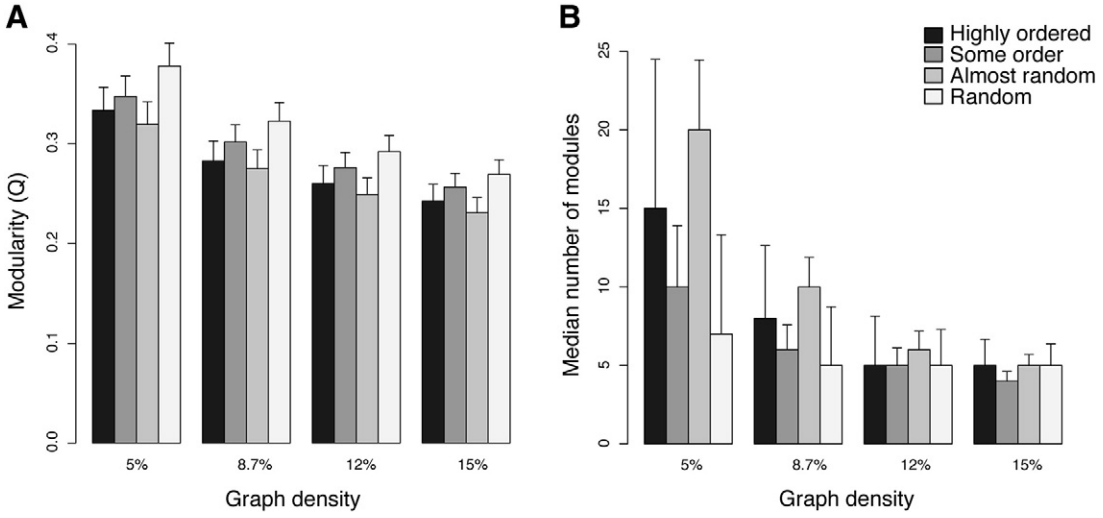

Fig. 3. Modularity in the four experimental conditions. Independent of graph density, modularity values (Q) patterned similarly across conditions (A) as did mean module number (B). Within each density level, modularity (Q) differed significantly across the 4 conditions. The mean number of modules differed for the 5%, 12%, and 15% edge density thresholds. Error bars here and in subsequent figures capture within-participant error (Loftus and Masson, 1994).

Modularity and module features

Network modularity across conditions

As a validation analysis, we first verified that brain network modularity derived from the experimental data exceeded that of matched null networks (following Meunier et al., 2009; Bassett et al., 2011). We found this was the case for all conditions (for each of the 4 conditions against the matched null network: Wilcoxon signed rank test, $Z = -4.62$, $p < .00001$ with participants as unit of variance).

We found that network modularity (Q) varied significantly across the 4 experimental conditions, independently of the edge density criterion used to threshold the connectivity matrix. The same relative pattern of Q values for the 4 conditions held across the different edge-density thresholds (see Fig. 3A). Modularity differed significantly across conditions for the 5% edge-density threshold (Friedman chi-square = 9.63, df = 3, $p < .05$), for the 8.7% threshold (Friedman chi-square = 9.13, df = 3, $p < .05$), for the 12% threshold (Friedman chi-square = 10.39, df = 3, $p < .05$), and for the 15% (Friedman chi-square = 8.24, df = 3, $p < .05$). In all cases, Q was highest for the Random condition (Fig. 3A). This is important because it showed that the experimental conditions impacted modularity, in a similar pattern, across a meaningful range of edge densities.

For the number of modules we found the converse pattern: the number of modules varied by condition and was lowest for the Random condition (Fig. 3B). The impact of condition on module number was significant at the 5% edge density threshold (Friedman chi-square = 14.74, df = 3, $p = .005$) and 12% density threshold (Friedman chi-square = 9.61, df = 3, $p < .05$), marginal at the 15% threshold (Friedman chi-square = 6.80, df = 3, $p = .078$), and not significant at the 8.7% threshold (Friedman chi-square = 5.01, df = 3, $p = .17$). We note that in the current data, there wasn't a necessary correlation between module number and modularity strength: from the sets of permutations we obtained 7600 sets of these two values, and the Pearson's R correlation between the two was negligible; −0.02.

Given these results for modularity strength and module number, for computational simplicity and clarity of this report we carried out our further analyses using the 5% edge density threshold. Across participants, this 5% density threshold gave medians of 10,880 nodes (1st quartile: 10,520, 3rd quartile: 11,070, SD = 885) and 2,961,000 edges (1st quartile: 2,821,000, 3rd quartile: 3,107,000, SD = 487,490).

Given our focus on the two extreme conditions in the subsequent analyses of module partition similarity and reorganization, we also examined whether the Highly ordered and Random conditions differed significantly in modularity. We found that they did (Wilcoxon signed rank test, $Z = -2.21$, $p < .05$).

Partition similarity

The global similarity of partitions between the Random and Highly ordered conditions was calculated using the Adjusted Rand Index and Normalized Mutual Information. The non-stationary aspect of the partition-finding modularity algorithm imposes an upper bound on similarity, since even the similarity of two partitions derived from the same connectivity matrix will be below unity. As detailed in the Methods section, to adjust for this stochasticity network partition similarity was estimated multiple times between the Random and Highly ordered conditions to yield a distribution of similarity values. We compared the resulting distribution to a sampling distribution that established an upper-bound limit, consisting of partition similarity values derived from a single condition's binarized connectivity matrix.

Fig. 4 shows the results of this analysis. First, even when partition pairs were derived from a single matrix of one condition (establishing the null distribution), similarity varied greatly, in line with prior indications of modularity optimization's non-unique solutions (Fortunato and Barthelemy, 2007; Lancichinetti and Fortunato, 2012; Muller and Meyer, 2014). Notwithstanding, it was still the case that partition similarity *across* the Random and Highly ordered conditions was much lower than that seen for the null distribution (Fig. 4A), indicating that the experimental conditions strongly impacted the modular partition structure. Specifically, across conditions, Adjusted Rand Index values centered at ~0.25, whereas within a condition it centered ~0.75, and these two distributions differed significantly (Kolmogorov–Smirnov test, D = 1, $p < .00001$). A very similar result was obtained using Normalized Mutual Information to quantify partition similarity (Fig. 4B; Kolmogorov–Smirnov test, D = 1, $p < .00001$).

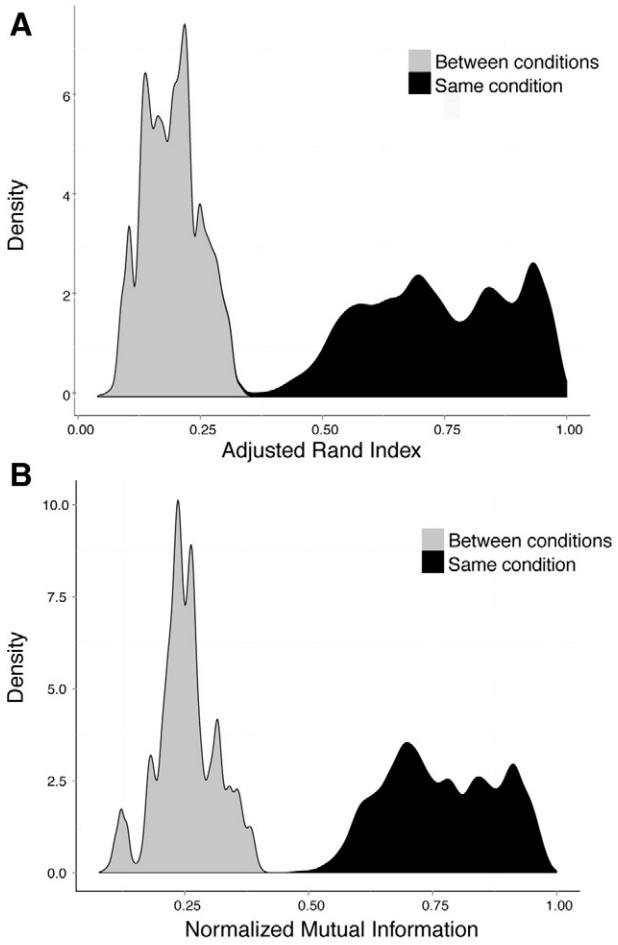

Fig. 4. Partition similarity of functional networks in the Random and Highly ordered conditions. Due to the stochastic nature of the modularity optimization algorithm, between-condition partition similarity is presented via a distribution (gray) and compared to a null distribution constructed from single matrix (black). A: Adjusted Rand Index values. B: Normalized Mutual Information values. For both measures, the null distribution differed significantly from that found for the comparison of the two conditions (both Kolmogorov–Smirnov tests, D = 1, $p < .00001$).

Distributions of node degree

Consistent with prior findings (Achard et al., 2006; Bassett et al., 2006; Fornito et al., 2010; Hayasaka and Laurienti, 2010), an exponentially truncated power law provided a good fit to the degree distributions. We obtained parameter estimates for the power law exponent (α) degree cutoff point (k_c), and coefficient (A) parameters per participant per condition and analyzed them at a group-level. Model fits at the single participant level were good, with most R^2 values exceeding 0.8. More importantly, these parameters all differed between conditions (power law exponent α: Friedman chi-square = 12.79, df = 3, $p = .005$; degree cut-off point k_c: Friedman chi-square = 12.28, df = 3, $p = .006$; and power law coefficient A: Friedman chi-square = 12.28, df = 3, $p = .006$). While there was no monotonic pattern, Fig. 5 depicts marked divergence in these parameter values across conditions. Notably, the Random condition showed the lowest cutoff, indicating relatively fewer nodes with a large number of connections.

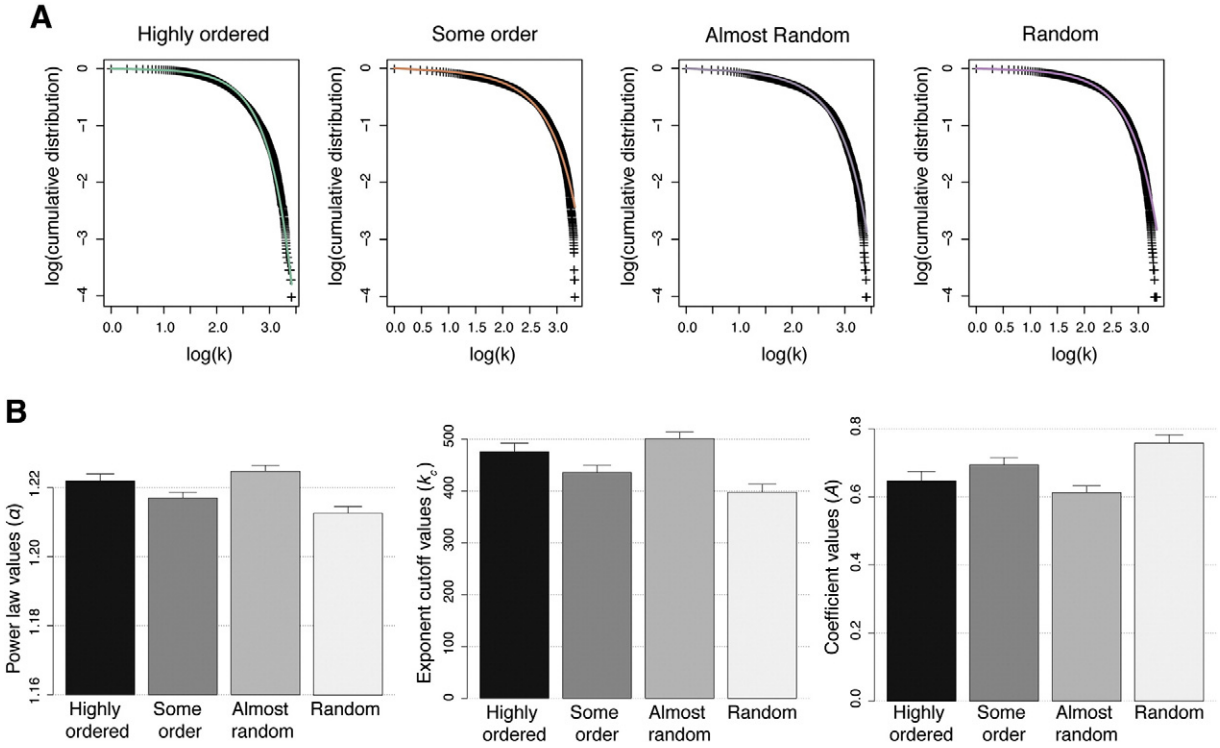

Fig. 5. Parameter estimates and aggregate plots for degree distributions by condition. A. Log–log plot of the cumulative degree distribution by condition for a randomly chosen participant. Colored lines in each condition depict fit of an exponentially truncated power law to the data. B. Best-fit parameter estimates for an exponentially truncated power law distribution were estimated per participant per condition and analyzed at the group level. These parameters differed significantly across conditions, and the Random condition had the lowest cutoff point, representing a degree distribution that held fewer voxels with high numbers of connections.

Single node set consistency

Our analyses to this point showed that the Random and Highly ordered conditions were associated with different modularity strength, number of modules, and with a qualitative change to network structure. Here we examined the extent to which single nodes maintained their modular grouping in these two conditions, by quantifying for each node, the proportion of its within-module connections in the Random condition that were also within-module connections in the Highly ordered condition (single node set consistency; SNSC, see Materials and methods).

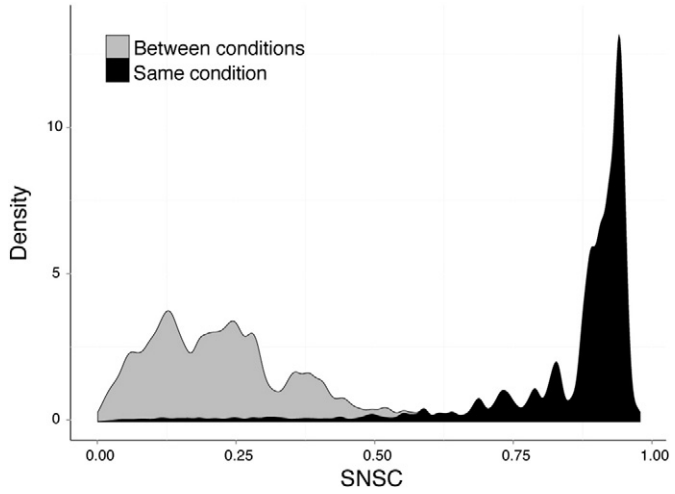

Fig. 6. Single node set consistency (SNSC) across the Random and Highly ordered conditions. SNSC is a node-level measure of the proportion of within-module connections that maintain across two partitions. Due to the stochastic nature of the modularity optimization algorithm, between-condition SNSC is presented via a distribution (gray) and compared to a null distribution constructed from single matrix (black). The gray distribution shows SNSC values when evaluating partitions constructed from the Random and Highly ordered conditions of the participant group. The black distribution is the null distribution and is derived from pairs of partitions generated from the same binarized matrix. The difference between distributions was significant (Kolmogorov–Smirnov test, D = .93, $p < .00001$), indicating considerably less stability in node-level connectivity across conditions compared to the within-condition null distribution.

Fig. 6 shows the main finding via a density plot of group-level SNSC values. The median value slightly exceeded 0.2, with very few nodes reaching values of 0.5, suggesting a strong shift of within-module connectivity across the two conditions. Given that the modularity partition-finding algorithm can produce different partitions — even when applied to the same matrix (and hence SNSC values < 1 by definition) — we also derived a null distribution of SNSC values by calculating SNSC values from partitioning pairings drawn from a single condition (see Materials and methods). As shown in Fig. 6, the modal value of this null distribution was 0.94, approaching unity. A formal test showed that the distribution of SNSC values across conditions was significantly lower than the sampling distribution of SNSC values (Kolmogorov–Smirnov test, D = .93, $p < .00001$). Thus, the Random and Highly ordered conditions were associated with significant change to within-module connectivity on the single node level.

Fig. 7 plots the median SNSC value of each node across participants. As shown in the figure, areas with relatively higher SNSC values were primarily within two networks: (1) the DMN, which includes anterior and posterior midline regions, as well as the inferior parietal lobule (IPL) and anterior superior temporal sulcus (STS), and (2) primary and secondary sensory regions. In contrast, dorso-lateral prefrontal areas bilaterally showed relatively lower values, suggesting more context-dependent roles for these areas (e.g., as described by Cole et al., 2013).

Changes in global connectivity

Using a whole brain analysis (controlled for family-wise error using cluster-based thresholding; see Materials and methods), we identified brain areas where voxels' mean global connectivity tracked regularity

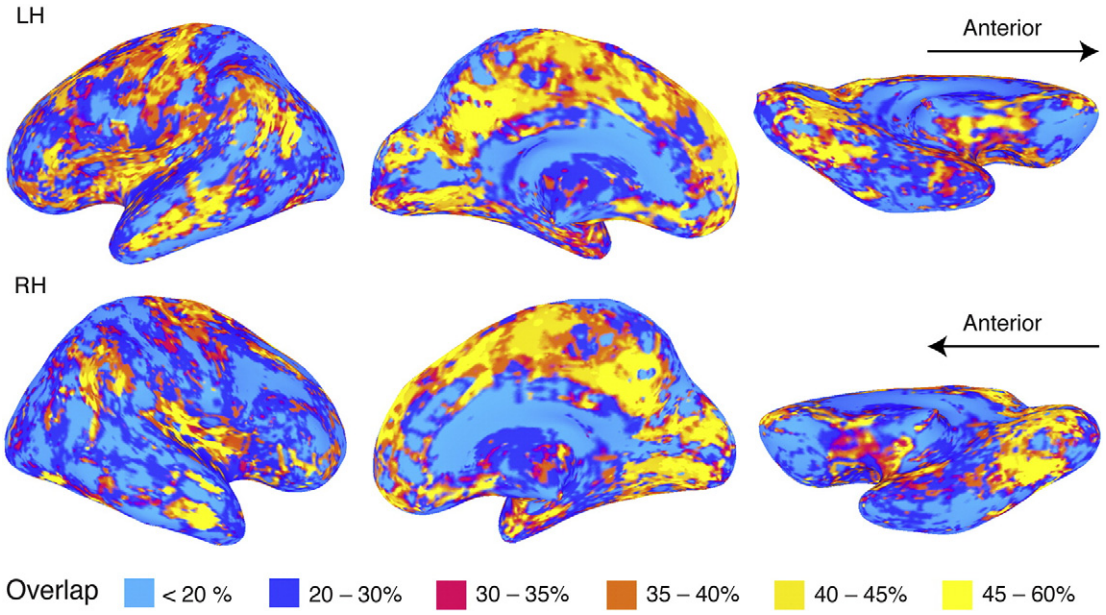

Fig. 7. Group-median single-node set consistency (SNSC) values at the single-node level. Warmer colors (higher SNSC) indicate voxels that maintain stronger module membership across the Random and Highly ordered conditions. Note that all values were much lower than the upper limit on SNSC values, which approached unity, as seen in Fig. 6. LH: left hemisphere. RH: right hemisphere.

in a linear or curvilinear pattern. The results are reported in Fig. 8, and cluster details are given in Table 1. Several regions were identified, and in all cases these showed lower connectivity in the Random than Highly ordered condition. The identified regions were mainly frontal ones, including bilateral middle and superior frontal gyri, as well as superior sections of supplementary motor areas. Linear trends were also found in the basal ganglia, most prominently in the left putamen, the left anterior and right pulvinar and medial–dorsal thalamic nuclei. In addition, we found two different cerebellar clusters, with extents in both cerebellar hemispheres.

Autonomic indices

We found no relation between the experimental conditions and autonomic (cardiac and respiratory) indices recorded during scanning. The mean heart rate in all conditions was 62–63 BPM (Mean/SD for

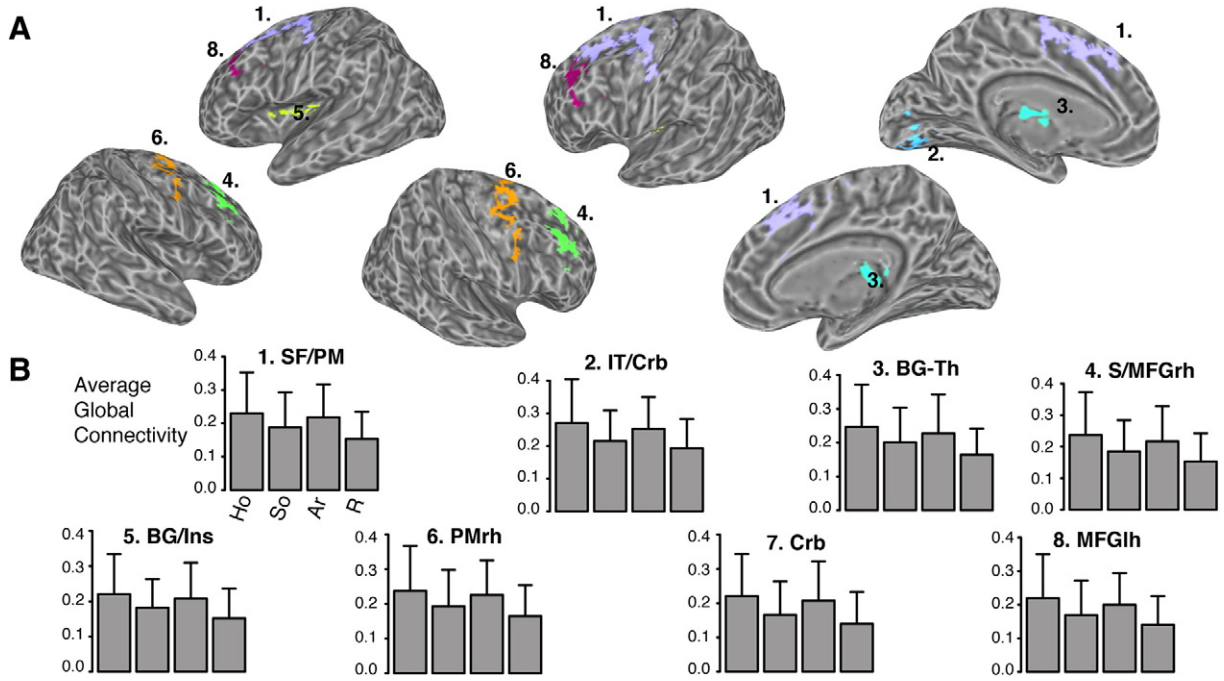

Fig. 8. Areas where average global connectivity decreased as condition disorder increased. A. Significant clusters where average connectivity strength (average functional connectivity of each voxel to every other voxel; Cole et al., 2010) decreased with input disorder (individual voxel $p < .01$, FWE $p < .05$). B. Corresponding graphs for clusters in A. Ho: Highly ordered, So: Some order, Ar: Almost random, R: Random. SF/PM: superior frontal/premotor, IT/Crb: inferior temporal/cerebellum, BG–Th: basal ganglia–thalamus, S/MFGrh: superior/middle frontal gyrus right hemisphere, BG/Ins: basal ganglia/insula, PMrh: premotor right hemisphere, Crb: cerebellum (not shown in Panel A), MFGlh: middle frontal gyrus left hemisphere.

Table 1
Details for significant clusters where voxel-level global connectivity varied by condition.

Cluster	Volume	CM RL	CM AP	CM IS	Mean	SEM	Max Int	Max Int RL	Max Int AP	Max Int IS
1	829	15.6	−4.8	49.4	3.2775	0.0125	5.06	10	4	58
2	395	−0.6	71.6	−20.2	3.328	0.0201	5.018	−6	70	−24
3	296	−3.6	15.6	11.3	3.2375	0.0174	4.325	−20	22	14
4	233	−29.9	−31.1	39.4	3.2448	0.0199	4.678	−34	−32	42
5	198	28.4	7.5	5.9	3.2944	0.0248	4.501	28	16	8
6	198	−32.3	4.5	54	3.1888	0.0172	4.039	−26	4	60
7	164	33.6	51.5	−32.2	3.5036	0.0413	5.267	32	52	−34
8	154	31.2	−25.9	33.1	3.1785	0.0199	4.341	36	−32	32

Note. The table provides information about the clusters depicted in Fig. 8. Cluster numbers (leftmost column) correspond to cluster numbers in Fig. 8. CM = center of mass. RL = right/left. AP = anterior/posterior. IS = inferior/superior. Max Int = Maximum Intensity (T value) for the linear contrast in the cluster. MNI coordinates, order RAI. Single voxel volume: 8 μl.

highest to lowest entropy condition: 62.7/9.5; 62.3/8.6; 62.7/10.1; 62.5/92). Heart rate variance (standard deviation of inter beat intervals) was also highly similar across conditions (arbitrary units, all values within 49–50). The similarity of these profiles across conditions, and removal of the variance associated with them from the BOLD signal, suggests that functional connectivity differences were not due to potential confounds between autonomic state and experimental condition.

Discussion

We found that global features of whole-brain network connectivity changed with simple manipulations of input regularity, in absence of any task demands. These global features included modularity strength, number of modules, partition structure, and features of node degree distributions. In addition, we demonstrated that alongside these large-scale changes there was considerable heterogeneity in the extent to which connectivity re-organized at the single node level, with sensory and default mode regions most resilient to environmental changes. In what follows we discuss these findings in relation to prior work.

The scope and triggers of contextual impact

The changes we documented to global network features were systematic across individuals, as indicated by highly statistically significant trends at the group level. This is a crucial finding because it is completely plausible that contextual manipulations could strongly impact network organization at the single-participant level, but in a manner that varied strongly and *in*consistently across individuals, resulting in null group-level results. Thus, large-scale functional networks not only flexibly and spontaneously reorganize with context, but they do so in a similarly patterned manner across individuals.

Our findings expand on prior work by showing that changes to network structure can be triggered without changes to physical features of stimuli or task. While strong manipulations of experimental state (e.g., rest vs. movie viewing; Moussa et al., 2011), task demand (Ekman et al., 2012), or cognitive state (e.g., sleep vs. rest; Uehara et al., 2013) clearly affect connectivity, our study shows those are not necessary for achieving such an impact, as our conditions were devoid of executive demands and required only passive listening.

It is interesting that our relatively simple experimental manipulation was sufficient to induce large-scale topographic changes, whereas several prior, ostensibly stronger manipulations in the literature indicated above did not document similar changes. One reason may be that the manipulation of input-regularity impacts multiple cognitive processes. Despite maintaining the same sensory/physical features across conditions, this manipulation has been shown to impact people's propensity to generate task-unrelated thoughts during listening and their affective appraisal of the stimuli (e.g., Vitz, 1964, 1966; Antrobus, 1968). Thus, although subtle, this manipulation likely impacts multiple brain systems, including those related to mind wandering (Mason et al., 2007), anxiety (Hirsh et al., 2012), or input prediction (Tobia et al., 2012).

The relation between input regularity and large-scale connectivity

The changes in global connectivity features we observed between the Highly ordered and Random condition may be due to the fact that the highly ordered stimulus we used, which contained stationary regularities, licensed prediction and instantiated long-range functional connectivity between frontal and sensory regions (Summerfield et al., 2006a, 2006b). Conversely, the strongest modularity found for the Random condition may reflect reduced communication between sensory and frontal systems, with relatively weaker information exchange. Such a balance is sensible from the perspective of an organism that optimizes resources dedicated to top-down processing (when predictions are licensed) vs. bottom-up processing (when inputs are noisy and anticipatory processes are less effective). Our node-level global connectivity analysis supports this possibility as it identified several regions where functional connectivity was lowest for the Random condition. Similar to prior work (Bassett et al., 2006; Fornito et al., 2010; Hayasaka and Laurienti, 2010), we modeled degree distributions with a truncated power law, here separately fitting each participant's data to draw conclusions on the group level. We found that the degree distributions' parameters differed by condition, with the random condition showing the lowest proportion of nodes with high degrees.

It has been shown that modularity strength provides little information about the underlying partition structure as solutions with very similar modularity values can differ greatly in their partition structure (Good et al., 2010). To evaluate whether the differences in modularity strength were accompanied by changes to partition structure we analyzed the similarity of partitions found for the Random and Highly ordered conditions. We found that these partitions were significantly less similar than would be expected by chance.

While several of our analyses focused on the contrast between the Highly ordered and Random conditions, it was not the case that there was a monotonic relation between input regularity and network modularity. For the number of modules in each condition, the Random condition was associated with the smallest number of modules, the Almost random condition with the largest number, and the other two conditions falling in between (for 5% and 8.7% densities). For the features of degree distributions, global connectivity, and modularity strength, the Almost random condition resembled the Highly ordered condition more than the Random condition. There could be a number of reasons for this non-monotonic relation. In general, a non-monotonic relation between any parameter of interest and input entropy can be explained by a basic tenet of complexity science, which is that both totally ordered and random inputs are less complex than inputs with mid-levels of disorder, in the sense that it is quite simple to abstractly represent the system/machine/generator producing ordered and random inputs but more difficult to represent the systems producing inputs with mid-

levels of disorder (see Nastase et al., 2015 for discussion in relation to neuroimaging data). In this approach, the Highly ordered and Random condition should resemble each other and diverge from the mid-level conditions. This pattern, however, was not found for any of the global features we examined in the current study, or for the whole-brain global connectivity analysis (but see Nastase, 2015 for such patterns when examining whole-brain connectivity of ACC and Hippocampus in these conditions). As mentioned above, the differences documented between the Random and Highly ordered conditions could reflect different types of processing associated with these conditions.

The results found for the Almost random condition are more difficult to interpret. To better understand this condition, we conducted a follow up analysis that examined the partition structure in this condition in relation to the other three conditions. This analysis indicated that the partition structure of the Almost random condition was *not* more similar to the Highly ordered condition than to the other two conditions.[1] Given that this condition was associated with a larger number of modules and lowest modularity (Fig. 3), a larger number of nodes with high node degree (Fig. 5b), and also stronger global connectivity than the Somewhat ordered condition (Fig. 8), we consider that these findings may be due to a particularly taxing cognitive demand that it poses. First, the minimal amount of redundancy in that condition may have instantiated a highly demanding learning situation, wherein participant's "second level" certainty about the degree of uncertainty was low. In other words, for this condition, not only was input uncertainty high, but the presence of infrequently-occurring short patterns could have made it difficult to computationally determine whether or not the input should be treated as random. Second, while this condition also formally allowed prediction, it lacked a single dominant transition constraint (and in this sense differed from the Highly ordered and Somewhat ordered conditions). Thus, even if the transition probabilities were learned, in order to use them, participants would need to entertain 2 equally probable transitions (each of 37.5%, see Fig. 1) given each stimulus.

The relation between input regularity and single-node connectivity: SNSC and global connectivity

One of our assumptions was that global changes in modularity could obscure a nuanced pattern, where some nodes maintain within-module connections across conditions and some do not. We derived a node-level measure (SNSC) that quantified each node's proportion of within-module connections in the Random condition that maintained in the Highly ordered condition. Because our nodes had relatively high spatial resolution, we could characterize variations in connectivity rearrangement across the brain with relatively good precision. We found that areas predominantly in prefrontal, motor, and somatosensory cortices were least likely to hold consistent modular connectivity. In contrast, DMN areas, including anterior and posterior medial regions, as well as the IPL, anterior STS, and primary sensory cortices showed relatively stable intra-modular connectivity between conditions. This pattern of results is highly consistent with those of Mennes et al. (2013). That study quantified the extent to which different brain regions maintained their connectivity profiles across different tasks. It found that subcortical and limbic regions, as well as motor and primary sensory cortices showed only moderate similarity in functional network correspondence, whereas DMN regions showed much stronger correspondence in network structure across tasks, suggesting the latter are less sensitive to specific task features (see also Golland et al., 2007)

A voxel's global connectivity is a measure independent of SNSC. In analyzing this measure, we found several cortical and subcortical areas where mean connectivity varied with condition so that connectivity was highest for the Highly ordered condition. The regions implicated were mainly superior and middle frontal regions bilaterally, with a noted absence of lateral temporal cortex regions implicated in auditory processing per se. We also found connectivity changes sub-cortically; sequencing-related operations in auditory streams has been linked to the putamen (Geiser et al., 2012; Grahn and Rowe, 2013), SMA, and lateral thalamus (Janata and Grafton, 2003).

Implications for the function versus structure debate

The functional or effective connectivity of brain network organization has been argued to adhere to core intrinsic, structural constraints (white-matter connectivity), as suggested by empirical work (e.g., Hagmann et al., 2008; Honey et al., 2009) and supported by computational simulations (e.g., Ghosh et al., 2008; Deco et al., 2009). A relation between structural and functional connectivity is also supported by work suggesting that brain networks organize with a stable, core topology (Cole et al., 2014). This topology has been said to reflect an intrinsic organization, with large-scale network features that maintain throughout active task and rest states.

An issue of increasing scrutiny, however, is to what extent the brain's functional organization is flexible. In particular, this issue pertains to understanding possible relations between the modularity of functional networks and structural connections (Sporns, 2013). One suggestion is that modularity reflects structural constraints that "promote functional segregation by forming local network communities that are intrinsically densely connected and strongly coupled" (Sporns, 2013, p. 162). In evaluating this issue, Messe et al. (2014) used simulations and concluded that the structural core forms a 'backbone' for functional connectivity. Importantly, however, their findings also indicated that functional connectivity manifested non-stationary dynamics, for which structural models did not explain a large portion of variance. Our results contribute to clarifying this issue, as they are the first to show that multiple core network features — including modularity — vary across implicit environments. It is important to point out that we used a highly conservative permutation-based method to derive representative modularity values on the single participant level in order to draw population-level conclusions. Our results are thus a strong complement to other work that showed flexible large-scale network topographies in task contexts (e.g., Wang et al., 2012; Bray et al., 2014).

Summary

During natural sensory perception individuals are exposed to multiple types of temporally unfolding environments that vary in regularity. We show that such environments are associated with changes to core global features of whole-brain connectivity. Although prior work has shown that experimental manipulations impact functional connectivity patterns, prior findings on the impact of external context on modularity were inconsistent. Our current results strongly suggest that, even in absence of task demands, temporal features of context can strongly impact modularity and other global features of whole-brain network connectivity. Our work also highlights the importance of understanding global changes in topology in tandem with finer-scale examinations, at the node and regional level. Finally, our work suggests that the modularity of functional networks, while likely constrained by structural connections, is not completely determined by the latter, and that the environment can introduce systematic changes to their configuration.

Conflict of interest statement

None.

[1] We calculated, on the single participant level, the pairwise similarity of the partition structure in this condition against each of the other three other conditions, using an NMI measure. We conducted a group level test on these values, and we found no significant differences in similarity ($ps > 0.15$).

Acknowledgments

This work was supported by the European Research Council Under the 7th Framework Starting Grant Program; Contract grant number: 263318 to U.H, and supported in part by funding from the Fondazione Cassa di Risparmio di Trento e Rovereto. We thank Sarah Kenny for developing the R implementation of brain connectivity analysis tools, Ben Davis for technical assistance, K.B. Bryant for moral fortitude and Mark Makers for gracious insights.

References

Achard, S., Salvador, R., Whitcher, B., Suckling, J., Bullmore, E., 2006. A resilient, low-frequency, small-world human brain functional network with highly connected association cortical hubs. J. Neurosci. Off. J. Soc. Neurosci. 26, 63–72.

Antrobus, J.S., 1968. Information theory and stimulus-independent thought. Br. J. Psychol. 59, 423–430.

Bassett, D.S., Meyer-Lindenberg, A., Achard, S., Duke, T., Bullmore, E., 2006. Adaptive reconfiguration of fractal small-world human brain functional networks. Proc. Natl. Acad. Sci. U. S. A. 103, 19518–19523.

Bassett, D.S., Wymbs, N.F., Porter, M.A., Mucha, P.J., Carlson, J.M., Grafton, S.T., 2011. Dynamic reconfiguration of human brain networks during learning. Proc. Natl. Acad. Sci. U. S. A. 108, 7641–7646.

Betti, V., Della Penna, S., de Pasquale, F., Mantini, D., Marzetti, L., Romani, G.L., Corbetta, M., 2013. Natural scenes viewing alters the dynamics of functional connectivity in the human brain. Neuron 79, 782–797.

Birn, R.M., Diamond, J.B., Smith, M.A., Bandettini, P.A., 2006. Separating respiratory-variation-related fluctuations from neuronal-activity-related fluctuations in fMRI. NeuroImage 31, 1536–1548.

Blondel, V.D., Guillaume, J.L., Lambiotte, R., Lefebvre, R., 2008. Fast unfolding of communities in large networks. J. Stat. Mech. Theory Exp. P10008.

Bray, S., Arnold, A.E., Levy, R.M., Iaria, G., 2014. Spatial and temporal functional connectivity changes between resting and attentive states. Hum. Brain Mapp. 36, 549–565.

Bullmore, E.T., Bassett, D.S., 2011. Brain graphs: graphical models of the human brain connectome. Annu. Rev. Clin. Psychol. 7, 113–140.

Chen, Z.J., He, Y., Rosa-Neto, P., Germann, J., Evans, A.C., 2008. Revealing modular architecture of human brain structural networks by using cortical thickness from MRI. Cereb. Cortex 18, 2374–2381.

Chow, H.M., Mar, R.A., Xu, Y., Liu, S., Wagage, S., Braun, A.R., 2014. Embodied comprehension of stories: interactions between language regions and modality-specific neural systems. J. Cogn. Neurosci. 26, 279–295.

Cole, M.W., Pathak, S., Schneider, W., 2010. Identifying the brain's most globally connected regions. NeuroImage 49, 3132–3148.

Cole, M.W., Reynolds, J.R., Power, J.D., Repovs, G., Anticevic, A., Braver, T.S., 2013. Multi-task connectivity reveals flexible hubs for adaptive task control. Nat. Neurosci. 16, 1348–1355.

Cole, M.W., Bassett, D.S., Power, J.D., Braver, T.S., Petersen, S.E., 2014. Intrinsic and task-evoked network architectures of the human brain. Neuron 83, 238–251.

Cox, R.W., 1996. AFNI: software for analysis and visualization of functional magnetic resonance neuroimages. Comput. Biomed. Res. 29, 162–173.

Danon, L., Diaz-Guilera, A., Duch, J., Arenas, A., 2005. Comparing community structure identification. J. Stat. Mech. Theory Exp. P09008.

Deco, G., Jirsa, V., McIntosh, A.R., Sporns, O., Kotter, R., 2009. Key role of coupling, delay, and noise in resting brain fluctuations. Proc. Natl. Acad. Sci. U. S. A. 106, 10302–10307.

den Ouden, H.E., Friston, K.J., Daw, N.D., McIntosh, A.R., Stephan, K.E., 2009. A dual role for prediction error in associative learning. Cereb. Cortex 19, 1175–1185.

den Ouden, H.E., Daunizeau, J., Roiser, J., Friston, K.J., Stephan, K.E., 2010. Striatal prediction error modulates cortical coupling. J. Neurosci. Off. J. Soc. Neurosci. 30, 3210–3219.

Doucet, G., Naveau, M., Petit, L., Zago, L., Crivello, F., Jobard, G., Delcroix, N., Mellet, E., Tzourio-Mazoyer, N., Mazoyer, B., Joliot, M., 2012. Patterns of hemodynamic low-frequency oscillations in the brain are modulated by the nature of free thought during rest. NeuroImage 59, 3194–3200.

Ekman, M., Derrfuss, J., Tittgemeyer, M., Fiebach, C.J., 2012. Predicting errors from reconfiguration patterns in human brain networks. Proc. Natl. Acad. Sci. U. S. A. 109, 16714–16719.

Fletcher, P.C., Zafiris, O., Frith, C.D., Honey, R.A., Corlett, P.R., Zilles, K., Fink, G.R., 2005. On the benefits of not trying: brain activity and connectivity reflecting the interactions of explicit and implicit sequence learning. Cereb. Cortex 15, 1002–1015.

Forman, S.D., Cohen, J.D., Fitzgerald, M., Eddy, W.F., Mintun, M.A., Noll, D.C., 1995. Improved assessment of significant activation in functional magnetic resonance imaging (fMRI): use of a cluster-size threshold. Magn. Reson. Med. 33, 636–647.

Fornito, A., Zalesky, A., Bullmore, E.T., 2010. Network scaling effects in graph analytic studies of human resting-state FMRI data. Front. Syst. Neurosci. 4, 22.

Fornito, A., Harrison, B.J., Zalesky, A., Simons, J.S., 2012. Competitive and cooperative dynamics of large-scale brain functional networks supporting recollection. Proc. Natl. Acad. Sci. U. S. A. 109, 12788–12793.

Fortunato, S., Barthelemy, M., 2007. Resolution limit in community detection. Proc. Natl. Acad. Sci. U. S. A. 104, 36–41.

Geiser, E., Notter, M., Gabrieli, J.D., 2012. A corticostriatal neural system enhances auditory perception through temporal context processing. J. Neurosci. Off. J. Soc. Neurosci. 32, 6177–6182.

Ghosh, A., Rho, Y., McIntosh, A.R., Kotter, R., Jirsa, V.K., 2008. Noise during rest enables the exploration of the brain's dynamic repertoire. PLoS Comput. Biol. 4, e1000196.

Glover, G.H., Li, T.Q., Ress, D., 2000. Image-based method for retrospective correction of physiological motion effects in fMRI: RETROICOR. Magn. Reson. Med. 44, 162–167.

Golland, Y., Bentin, S., Gelbard, H., Benjamini, Y., Heller, R., Nir, Y., Hasson, U., Malach, R., 2007. Extrinsic and intrinsic systems in the posterior cortex of the human brain revealed during natural sensory stimulation. Cereb. Cortex 17 (4), 766–777.

Good, B.H., de Montjoye, Y.A., Clauset, A., 2010. Performance of modularity maximization in practical contexts. Phys. Rev. E Stat. Nonlinear Soft Matter Phys. 81, 046106.

Grahn, J.A., Rowe, J.B., 2013. Finding and feeling the musical beat: striatal dissociations between detection and prediction of regularity. Cereb. Cortex 23, 913–921.

Hagmann, P., Cammoun, L., Gigandet, X., Meuli, R., Honey, C.J., Wedeen, V.J., Sporns, O., 2008. Mapping the structural core of human cerebral cortex. PLoS Biol. 6, e159.

Hasson, U., Nusbaum, H.C., Small, S.L., 2009. Task-dependent organization of brain regions active during rest. Proc. Natl. Acad. Sci. U. S. A. 106, 10841–10846.

Hayasaka, S., Laurienti, P.J., 2010. Comparison of characteristics between region-and voxel-based network analyses in resting-state fMRI data. NeuroImage 50, 499–508.

Hirsh, J.B., Mar, R.A., Peterson, J.B., 2012. Psychological entropy: a framework for understanding uncertainty-related anxiety. Psychol. Rev. 119, 304–320.

Honey, C.J., Sporns, O., Cammoun, L., Gigandet, X., Thiran, J.P., Meuli, R., Hagmann, P., 2009. Predicting human resting-state functional connectivity from structural connectivity. Proc. Natl. Acad. Sci. U. S. A. 106, 2035–2040.

Hubert, L., Arabie, P., 1985. Comparing partitions. J. Classif. 2, 193–218.

Janata, P., Grafton, S.T., 2003. Swinging in the brain: shared neural substrates for behaviors related to sequencing and music. Nat. Neurosci. 6, 682–687.

Kitzbichler, M.G., Henson, R.N., Smith, M.L., Nathan, P.J., Bullmore, E.T., 2011. Cognitive effort drives workspace configuration of human brain functional networks. J. Neurosci. Off. J. Soc. Neurosci. 31, 8259–8270.

Kuncheva, L.I., Hadjitodorov, S.T., 2004. Using diversity in cluster ensembles. 2004 IEEE International Conference on Systems, Man and Cybernetics, pp. 1214–1219.

Lancichinetti, A., Fortunato, S., 2012. Consensus clustering in complex networks. Sci. Rep. 2, 336.

Loftus, G.R., Masson, M.E.J., 1994. Using confidence-intervals in within-subject designs. Psychon. Bull. Rev. 1, 476–490.

Mason, M.F., Norton, M.I., Van Horn, J.D., Wegner, D.M., Grafton, S.T., Macrae, C.N., 2007. Wandering minds: the default network and stimulus-independent thought. Science 315, 393–395.

Mennes, M., Kelly, C., Colcombe, S., Castellanos, F.X., Milham, M.P., 2013. The extrinsic and intrinsic functional architectures of the human brain are not equivalent. Cereb. Cortex 23, 223–229.

Messe, A., Rudrauf, D., Benali, H., Marrelec, G., 2014. Relating structure and function in the human brain: relative contributions of anatomy, stationary dynamics, and non-stationarities. PLoS Comput. Biol. 10, e1003530.

Meunier, D., Lambiotte, R., Fornito, A., Ersche, K.D., Bullmore, E.T., 2009. Hierarchical modularity in human brain functional networks. Front. Neuroinformatics 3, 37.

Moussa, M.N., Vechlekar, C.D., Burdette, J.H., Steen, M.R., Hugenschmidt, C.E., Laurienti, P.J., 2011. Changes in cognitive state alter human functional brain networks. Front. Hum. Neurosci. 5, 83.

Muller, A.M., Meyer, M., 2014. Language in the brain at rest: new insights from resting state data and graph theoretical analysis. Front. Hum. Neurosci. 8, 228.

Nastase, S.A., Iacovella, V., Davis, B., Hasson, U., 2015. Connectivity in the human brain dissociates entropy and complexity of auditory inputs. Neuroimage. 108, 292–300. http://dx.doi.org/10.1016/j.neuroimage.2014.12.048.

Nicol, R.M., Chapman, S.C., Vertes, P.E., Nathan, P.J., Smith, M.L., Shtyrov, Y., Bullmore, E.T., 2012. Fast reconfiguration of high-frequency brain networks in response to surprising changes in auditory input. J. Neurophysiol. 107, 1421–1430.

Patenaude, B., Smith, S.M., Kennedy, D.N., Jenkinson, M., 2011. A Bayesian model of shape and appearance for subcortical brain segmentation. NeuroImage 56, 907–922.

Preminger, S., Harmelech, T., Malach, R., 2011. Stimulus-free thoughts induce differential activation in the human default network. NeuroImage 54, 1692–1702.

Rand, W.M., 1971. Objective criteria for the evaluation of clustering methods. J. Am. Stat. Assoc. 66, 846–850.

Rubinov, M., Sporns, O., 2010. Complex network measures of brain connectivity: uses and interpretations. NeuroImage 52, 1059–1069.

Smith, S.M., 2002. Fast robust automated brain extraction. Hum. Brain Mapp. 17, 143–155.

Sporns, O., 2013. Network attributes for segregation and integration in the human brain. Curr. Opin. Neurobiol. 23, 162–171.

Stanley, M.L., Dagenbach, D., Lyday, R.G., Burdette, J.H., Laurienti, P.J., 2014. Changes in global and regional modularity associated with increasing working memory load. Front. Hum. Neurosci. 8, 954.

Summerfield, C., Egner, T., Greene, M., Koechlin, E., Mangels, J., Hirsch, J., 2006a. Predictive codes for forthcoming perception in the frontal cortex. Science 314, 1311–1314.

Summerfield, C., Greene, M., Wager, T., Egner, T., Hirsch, J., Mangels, J., 2006b. Neocortical connectivity during episodic memory formation. PLoS Biol. 4, e128.

Tobia, M.J., Iacovella, V., Davis, B., Hasson, U., 2012. Neural systems mediating recognition of changes in statistical regularities. NeuroImage 63, 1730–1742.

Uehara, T., Yamasaki, T., Okamoto, T., Koike, T., Kan, S., Miyauchi, S., Kira, J.I., Tobimatsu, S., 2013. Efficiency of a "small-world" brain network depends on consciousness level: a resting-state fMRI study. Cereb. Cortex 24, 1529–1539.

Uehara, T., Yamasaki, T., Okamoto, T., Koike, T., Kan, S., Miyauchi, S., Kira, J., Tobimatsu, S., 2014. Efficiency of a "small-world" brain network depends on consciousness level: a resting-state FMRI study. Cereb. Cortex 24, 1529–1539.

Vitz, P.C., 1964. Preferences for rates of information presented by sequences of tones. J. Exp. Psychol. 68, 176–183.

Vitz, P.C., 1966. Affect as a function of stimulus variation. J. Exp. Psychol. 71, 74–79.

Wang, Z., Liu, J., Zhong, N., Qin, Y., Zhou, H., Li, K., 2012. Changes in the brain intrinsic organization in both on-task state and post-task resting state. NeuroImage 62, 394–407.